Vertically Aligned N-Doped Coral-like Carbon Fiber Arrays as Efficient Air Electrodes for High-Performance Nonaqueous Li–O_2 Batteries

Jianglan Shui,[†] Feng Du,[†] Chenming Xue,[‡] Quan Li,[‡] and Liming Dai[†,*]

[†]Department of Macromolecular Science and Engineering, Case School of Engineering, Case Western Reserve University, 10900 Euclid Avenue, Cleveland, Ohio 44106, United States and [‡]Liquid Crystal Institute and Chemical Physics Interdisciplinary Program, Kent State University, Kent, Ohio 44242, United States. The manuscript was written through contributions of all authors. All authors have given approval to the final version of the manuscript.

ABSTRACT High energy efficiency and long cycleability are two important performance measures for Li–air batteries. Using a rationally designed oxygen electrode based on a vertically aligned nitrogen-doped coral-like carbon nanofiber (VA-NCCF) array supported by stainless steel cloth, we have developed a nonaqueous Li–O_2 battery with an energy efficiency as high as 90% and a narrow voltage gap of 0.3 V between discharge/charge plateaus. Excellent reversibility and cycleability were also demonstrated for the newly developed oxygen electrode. The observed outstanding performance can be attributed to its unique vertically aligned, coral-like N-doped carbon microstructure with a high catalytic activity and an optimized oxygen/electron transportation capability, coupled with the microporous stainless steel substrate. These results demonstrate that highly efficient and reversible Li–O_2 batteries are feasible by using a rationally designed carbon-based oxygen electrode.

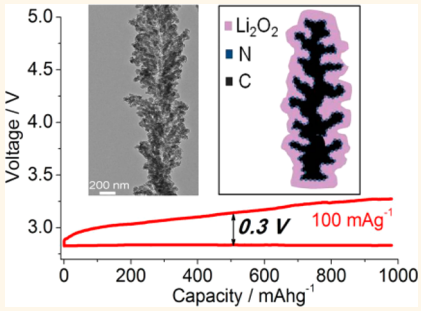

KEYWORDS: Li–air battery · oxygen electrode · carbon fiber · catalyst · electrochemistry

Li–O_2 batteries have recently emerged as high energy density devices with a theoretical energy density of ~3500 Wh kg^{-1}, nearly 8 times higher than that of commercial Li-ion batteries, and the ability to power electrical vehicles for a 500-miles range per charge.[1−8] A typical nonaqueous Li–O_2 battery is composed of three essential components: (1) a metallic lithium anode, (2) a porous cathode (usually carbon-based materials with or without catalysts), and (3) nonaqueous electrolyte (Li^+-containing solution) in between. The key charge/discharge reactions take place at the oxygen electrode, $2Li^+ + 2e + O_2 \leftrightarrow Li_2O_2$, with a thermodynamic potential of 2.96 V.[9] During discharging, oxygen molecule is reduced by electrons from the current collector to combine with Li^+ ions dissolved in the electrolyte to produce solid Li_2O_2 on the cathode.[10] Subsequent charging causes a reverse reaction. However, huge polarizations are commonly observed during charging, with a typical 1–2 V voltage gap between the charge and discharge plateaus.[11−13] Because of the instability of nonaqueous electrolytes, the decomposition of electrolytes to form an insulating coating on the electrode surface increases the overpotential, which, in turn, accelerates the decomposition of electrolytes.[12,14−18] So far, no stable nonaqueous electrolyte has been found. Besides, carbon materials in oxygen electrodes have been proven to decompose accompanying the electrolyte decomposition, particularly at high overpotentials.[19−23] On the other hand, the poor electron transportation between the electrode and Li_2O_2, due to the charging-induced formation of the Li_2O_2/electrode interfacial barrier,[7,24−27] contributes also to the high polarizations for nonaqueous Li–O_2 batteries. Various approaches have been developed to address these problems, including the use of different catalysts,[28−35] redox mediators in electrolytes,[24] and oxygen electrodes with optimized microstructures.[7,26,36] These efforts have improved energy efficiencies (defined by the percentage of discharge voltage over charge voltage at the middle

* Address correspondence to liming.dai@case.edu.

Received for review January 17, 2014 and accepted February 25, 2014.

Published online February 25, 2014
10.1021/nn500327p

of the charge/discharge plateaus) from 50 to 70% for Li−O_2 batteries in the last couple of years.

Generally speaking, an ideal oxygen electrode requires a highly conductive porous structure to facilitate both electron and oxygen transportations. A large specific surface area is also desirable for the electrode to show a high Li_2O_2 uptake. Among various oxygen electrodes, fibrous electrodes, including carbon fibers,[37] carbon nanotubes,[36,38−45] tubular polypyrrole,[26] and manganese oxide nanowires,[46] have been exploited for efficient electron and oxygen transportations. However, most fibrous electrodes still suffered from multiple drawbacks. For instance, spherical shaped Li_2O_2 particles often grow on the fiber surface with a very limited contact to the conductive substrate,[27,36,37] while a homogeneous coating layer of Li_2O_2 over the electrode material is more favorable than separated large particles for a uniform electrochemical reaction on the electrode. Very recently, noncrystalline Li_2O_2 has been demonstrated to form on multiwall CNTs decorated with noble metal catalysts with the catalytically functionalized fiber surface to facilitate the oxygen reduction reaction (ORR) all over the fiber surface.[43] The continuous coating layer of Li_2O_2 over the electrode material was found to be also favorable for the subsequent oxygen evolution reaction (OER) because the improved contact between the electrode and Li_2O_2 led to a low overpotential.[43,45] Although recent efforts have reduced the voltage gap between charge/discharge plateaus from 1.5 to 0.7 V and extended the number of reversible cycles up to 100,[13,29,35,42,45,47,48] oxygen electrodes (including fibrous ones) that simultaneously possess a high specific capacity, high energy efficiency, and long cycling life are still scarce.

In this work, vertically aligned nitrogen-doped coral-like carbon nanofiber (VA-NCCF) arrays were prepared by chemical vapor deposition (CVD, Figure S1, Supporting Information) and then transferred onto a piece of microporous stainless steel cloth as a binder-free oxygen electrode for nonaqueous Li−O_2 batteries. A narrow voltage gap (0.3 V) between the charge and discharge plateaus and an unusually high energy efficiency of 90% were obtained. To the best of our knowledge, these are the lowest overpotential and the highest energy efficiency among the reported Li−O_2 batteries. More than 150 highly reversible cycles under a specific capacity of 1000 mAh g^{-1} were also demonstrated.

RESULTS AND DISCUSSION

Figure 1a shows a typical scanning electron microscopic (SEM) image for a VA-NCCF forest grown on a Si wafer with a thickness of ~20 μm and a density of ~20 μg cm^{-2}. The zigzag-like carbon fibers aligned normal to the substrate and slightly tangled with each other, leading to good conductivities for both the in-plane and through-thickness directions while providing a large free space within the layer for efficient

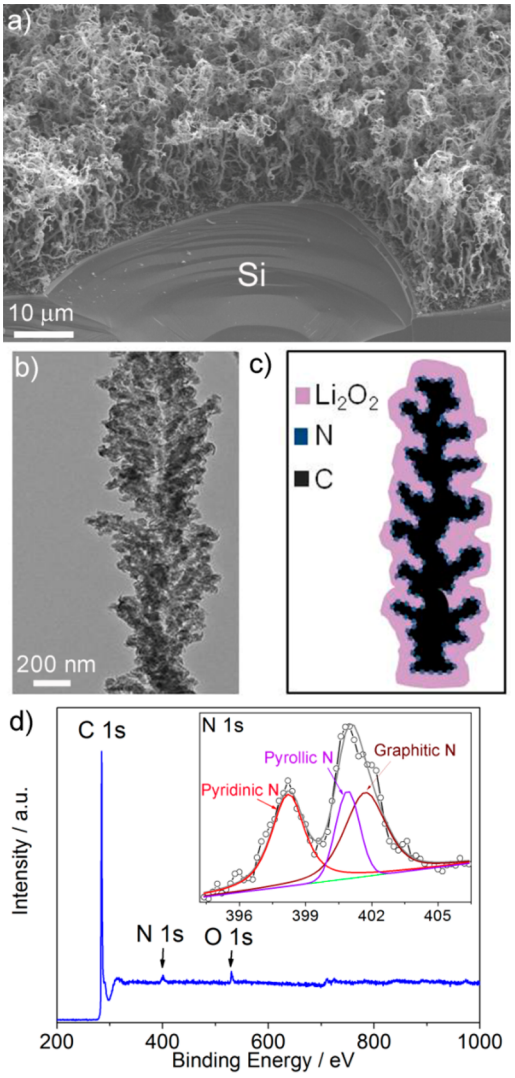

Figure 1. (a) SEM image of a VA-NCCF array grown on a piece of Si wafer by CVD. (b) TEM image of an individual VA-NCCF. (c) The sketch of Li_2O_2 grown on a coral-like carbon fiber, which has an advantage to tightly hold the Li_2O_2 deposit by the rugged surface (*cf.* Figure 3b,e). (d) An XPS survey spectrum of the VA-NCCF, and the insert is the corresponding high-resolution XPS spectrum of nitrogen.

oxygen/electrolyte transportation and a large uptake of Li_2O_2. The VA-NCCF electrode of a well-defined large surface area with all the nanofiber top-ends falling on one plane at the electrode/electrolyte interface can offer additional advantages to not only facilitate the electrolyte/reactant diffusion for current enhancement but also enhance the current transportation through the shortest pathway along the vertically aligned fiber length without the need of a binder. Binder-free electrode can reduce the electrical resistance, expose all active surface area to support the electrochemical process, and exclude all the possible side-effects associated with the binder decomposition.[49] A transmission electron microscopic (TEM) image of an individual fiber is given in Figure 1b, which shows the coral-like microstructure with many branches along the fiber

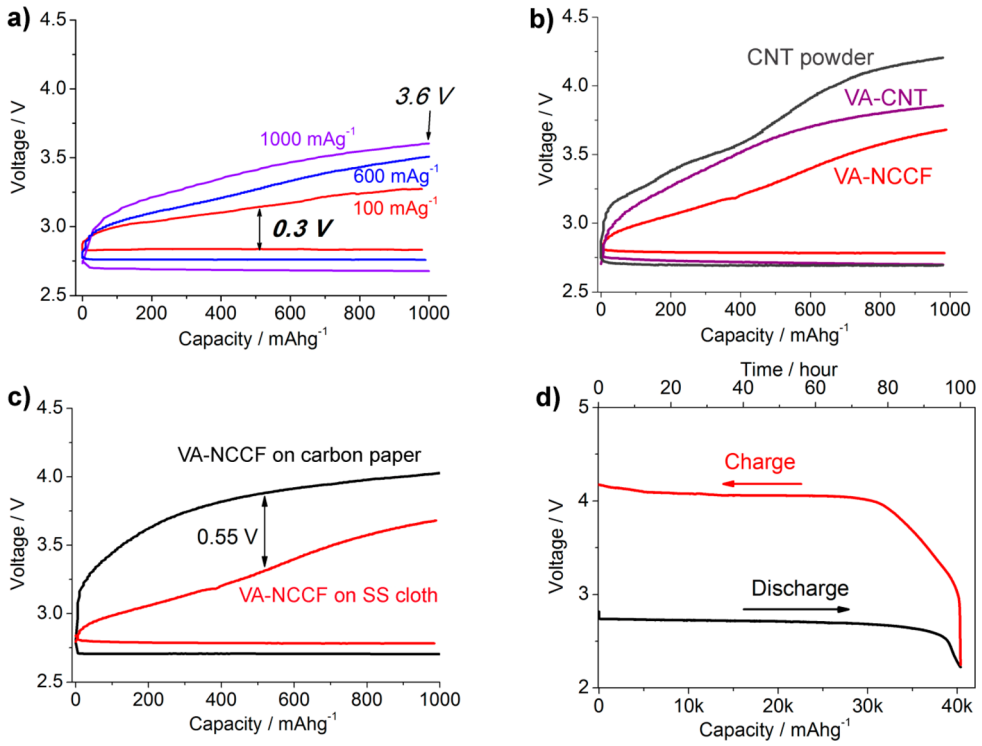

Figure 2. (a) Rate performance of the VA-NCCF electrode under current densities of 100, 600, and 1000 mA g^{-1}. (b) Comparison of the VA-NCCF with undoped vertically aligned carbon nanotubes (VA-CNT), and CNT powder. In all cases, a piece of microporous stainless steel (SS) cloth was used as the current collector. (c) The VA-NCCF forest on two different kinds of current collectors: the stainless steel cloth and Toray carbon paper. (d) Discharge/charge voltage profile of the VA-NCCF as the function of specific capacity. The cutoff voltages were 2.2 V for discharging and 4.4 V for charging. Current density was 500 mA g^{-1}.

"trunk" to enlarge the surface area, in respect with smooth (unbranched) carbon fibers or CNTs, for enhancing the electrode/electrolyte interaction and Li_2O_2 deposition over the whole surface of a branched fiber with a close electrical contact (*cf.* Figure 1c supported by Figure 3b,e).

The presence of structural nitrogen in the VA-NCCF was confirmed by X-ray photoelectron spectroscopic (XPS) measurements. The XPS survey spectrum given in Figure 1d shows the presence of 95.9 atom % of C, 1.0 atom % of O, and 3.1 atom % of N in the VA-NCCF sample. The oxygen incorporation is possibly due to physical adsorption from air, which is an additional advantage for ORR electrodes.[50] The absence of any obvious metal peak in the XPS survey spectrum suggests that most of the metal catalyst particles formed during the "base-growth" process have been left on the growth substrate after removal of the VA-NCCF forest and/or removed by the acid washing during the electrode preparation, as confirmed by the thermogravimetric analyses (Figure S2, Supporting Information). Therefore, the VA-NCCF electrode serves as carbon-based catalyst(s) for ORR/OER in this study (*vide infra*). The curve-fitted high-resolution XPS N 1s spectrum (inset of Figure 1d) shows the incorporation of pyridinic-like (~398 eV, ~40 atom % of the total nitrogen), pyrrolic-like (~401 eV, ~20 atom % of the total nitrogen), and graphitic (~402 eV, ~40 atom % of the total nitrogen) nitrogen atoms within the VA-NCCF sample. The presence of pyridinic and pyrrolic nitrogen atoms in unbranched carbon nanostructures have been demonstrated to be efficient catalytic sites for ORR in fuel cells[51−53] and Li−O_2 batteries.[32,47,54]

The VA-NCCF electrode was further characterized in Li−O_2 batteries with a piece of Li foil as anode and 1 M bis(trifluoromethane)sulfonimide lithium salt ($LiCF_3SO_3$) in tetraethylene glycol dimethyl ether (TEGDME) as electrolyte. Three freshly prepared batteries were tested separately under current densities of 100, 600, and 1000 mA g^{-1} at a controlled capacity of 1000 mAh g^{-1}. As shown in Figure 2a, a low overpotential of 0.3 V at the middle of discharge/charge plateaus was observed at the current density of 100 mA g^{-1}. The overpotentials were still reasonably low even when the current density was increased to 600 and 1000 mA g^{-1} with respect to a typical value of 1−2 V for other Li−O_2 batteries.[11−13] The cutoff voltage at the end of charge was just 3.6 V at the current density as high as 1000 mA g^{-1}. To the best of our knowledge, such a low overpotential (0.3 V) was the first time reported for nonaqueous Li−O_2 batteries, which is even lower than those of noble metal-based catalysts.[29,43,45,55] The corresponding energy efficiency was calculated to be 90%, the highest value for nonaqueous Li−O_2 batteries reported so far. The rate performance was also investigated for a single cell starting from the current

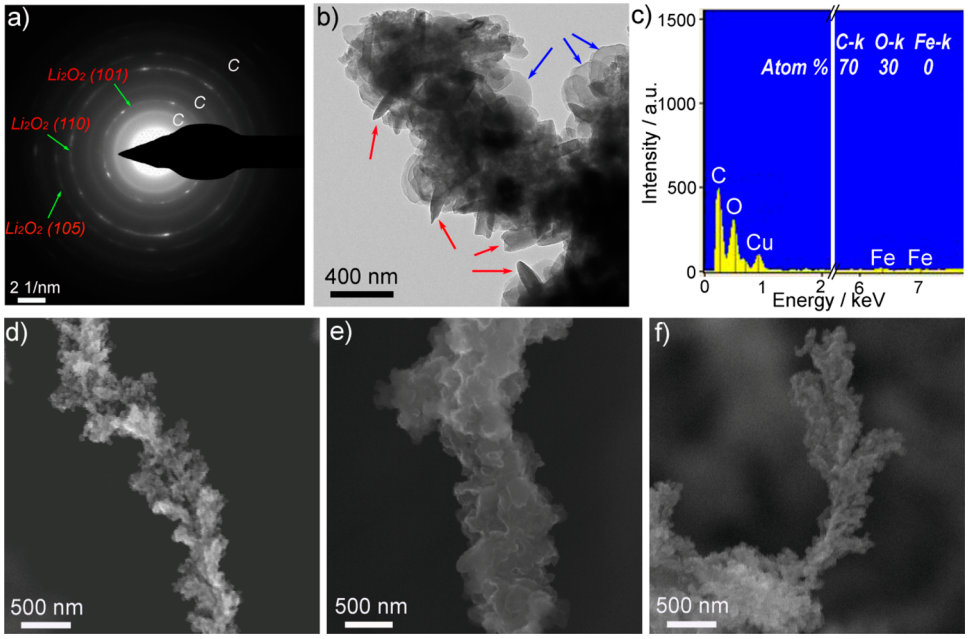

Figure 3. Identification of Li_2O_2 deposited on catalyst fiber by (a) the selected area electron diffraction (SAED) pattern of a discharged VA-NCCF fiber, and (b) TEM image of a discharged catalyst fiber (blue and red arrows indicate spherical- and spindle-shaped Li_2O_2 particles, respectively). (c) A spot-on EDX profile of the discharged fiber. The Li_2O_2 formation/decomposition during a round of discharge/charge cycle on the VA-NCCF fiber: SEM images of (d) the pristine fiber, (e) the discharged fiber, and (f) the charged fiber after predischarge. The discharge/charge capacities were controlled at 4000 mAh g^{-1}. Note that the mapping micrographs shown in (d), (e), and (f) were not taken from the same spot because of technical difficulties.

density of 100−1500 mA g^{-1} in five sequential cycles with a controlled capacity of 1000 mAh g^{-1}. In this case, the cutoff voltage was still found to be no more than 3.8 V at the end of the fifth charge under the current density of 1500 mA g^{-1} (Figure S3, Supporting Information).

To evaluate the factors related to the battery performance of the VA-NCCF array, we carried out the electrochemical measurements on undoped VA-CNT (Figure S4, Supporting Information) to illustrate the effect of N-doping, and nonaligned CNT powder to reveal the alignment effect on the cell performance. As seen in Figure 2b, the CNT powder exhibited the highest overpotential, followed by the VA-CNT, and VA-NCCF electrodes. The lower overpotentials for the aligned electrodes than that of the CNT powder could be attributed to the alignment-induced enhancement of mass/current transport described earlier. The VA-NCCF electrode showed the lowest overpotential due to the combined effect of the enhanced mass/current transport by alignment and the N-doping-induced catalytic activity.[51]

Possible effects of the current collector on the overpotential of the VA-NCCF electrode were also investigated. Carbon papers have been commonly used as the current collectors for the air electrode in Li−air batteries. However, we found in this study that the use of a piece of stainless steel (SS) cloth (supersmall particle-filtering stainless steel wire cloth, 304 stainless steel, 200 × 1400 mesh, purchased from McMaster-Carr) as the substrate and current collector for the VA-NCCF array could dramatically reduce the charge overpotential by 0.55 V at discharge−charge depth of 500 mAh g^{-1} and improve discharge overpotential by 0.1 V (Figure 2c), compared with hydrophobic carbon paper (Toray TGP-H-060, purchased from Fuel Cell Store). The improvement on discharge overpotential was not as much as that of charge process because the discharge voltage was already close to the thermodynamic potential 0.96 V. The carbon paper has pore sizes of ~100 μm, while the SS cloth has much smaller pores of ~10 μm to ensure a better contact to the catalyst array (Figure S5, Supporting Information). Besides, the 304 stainless steel has a much lower electrical resistivity of 0.07 mohm cm than that of the Toray carbon paper (80 mohm cm) to facilitate the electron transport. However, the SS cloth substrate itself has a very low surface area and a very high overpotential as an O_2 electrode. Therefore, the observed outstanding battery performance for the VA-NCCF electrode can be exclusively contributed to the aligned carbon fiber array (Figure S6, Supporting Information). By contrast, the carbon paper substrate is composed of micrometer-sized carbon fibers capable to act as an O_2 electrode.[47] To completely eliminate any possible effect of the current collector on the battery performance, we used the highly conductive and inert SS cloth, rather than the carbon paper, as the current collector for most of the subsequent measurements.

The full capacity of the VA-NCCF electrode was explored by discharging the cell down to 2.2 V at the current density of 500 mA g^{-1}, then charging to an

equivalent capacity at the same current density. A high capacity over 40 000 mAh g^{-1} was demonstrated after 100 h discharge (Figure 2d). During the subsequent charge processes, the first 10 000 mAh g^{-1} capacity was made under 4.0 V, and most of the rest capacity was recovered under 4.1 V. Since electrolyte decomposition could be accelerated at high voltages (*e.g.*, > 4.0 V), electrolyte decomposition, if any, might have contributed to the total capacity in this study. Compared with carbon black and carbon fibers,[12,37,39] however, the above results clearly indicate a larger specific capacity and a smaller charging overpotential for a full discharged/charged cycle. This, once again, can be attributed to the unique vertically aligned, coral-like, N-doped carbon microstructure with a large storage space, an optimized oxygen/electron transportation capability, and a high catalytic activity.

To identify the discharged product (Li_2O_2) and prove the cell rechargeability for a complete discharge/charge cycle, we performed the selected area electron diffraction (SAED) on a discharged fiber. Figure 3a shows the diffraction pattern for the VA-NCCF electrode, revealing the presence of crystalline Li_2O_2. The corresponding SAED pattern for the pristine VA-NCCF array shows diffusive rings for polycrystal carbon (Figure S7, Supporting Information). The TEM image of a discharged catalyst fiber shown in Figure 3b further revealed that the Li_2O_2 deposit composed mainly of spherical-, spindle-, and irregular shaped particles densely linked with each other along the catalyst fiber (see also Figures S8 and S9, Supporting Information).[35,56,57] The corresponding EDX analysis of the discharged fiber indicated about 30 atom % of oxygen and 70 atom % of carbon with virtually no iron but some copper from the TEM grid used for the sample preparation (Figure 3c). The presence of oxygen is mainly contributed by Li_2O_2, as only 1.0 atom % oxygen was detected by XPS analysis on the pristine fibers. However, possible contribution from electrolyte decomposition cannot be ruled out, albeit it is insignificant within a short time cycle for the efficient catalyst.

The formation/decomposition of Li_2O_2 during a discharge/charge cycle was followed further by SEM imaging, whereas its growth mechanism is beyond the scope of this study.[25,57,58] As expected, Figure 3d shows a coral-like structure with many branches for the pristine catalyst fiber. After a discharge (4000 mAh g^{-1}), the free space between branches along the fiber was almost completely filled by the discharge product, Li_2O_2 (Figure 3e). It is worthy to note that Li_2O_2 deposited densely along the coral-like fiber to fill up the entire interbranch space. The continuous deposition of Li_2O_2 presumably resulted from the homogeneous N-doping along the coral-like fiber. The observed morphology for the Li_2O_2 deposited on the VA-NCCF electrode is quite different from those on its counterparts based on unbranched carbon nanofibers or carbon nanotubes, which usually support the deposition of isolated individual particles.[36,37] As mentioned earlier,[43,45] the formation of the continuous Li_2O_2 coating can ensure a good electrical contact to reduce the electrochemical reaction barrier. The coral-like fiber structure reappeared (Figure 3f) after a recharging process at 4000 mAh g^{-1}, indicating the removal of Li_2O_2 coating by a reversible electrochemical process. Elemental mapping could further clearly demonstrate the Li_2O_2 formation in discharge and decomposition in the following charge processes (Figure S10, Supporting Information).

Because of the low overpotential of the VA-NCCF electrode, the electrolyte decomposition could be minimized, leading to a long device cycle life. To investigate the stability of the VA-NCCF electrode, we performed continuous charge/discharge cycling of one cell using the SS cloth substrate for more than two months and 150 cycles at a specific capacity of 1000 mAh g^{-1} per discharge/charge cycle. As can be seen in Figure 4a,b, the cell based on the SS-supported VA-NCCF electrode showed an almost constant capacity over 150 cycles, and the voltage profile was fairly stable with little change in overpotential after the 10th cycle (Figure 4b). Similar results were obtained for the VA-NCCF electrode using carbon paper as the current collector over more than 80 days cycling (Figure 4c,d), albeit with about 20−30 mV higher overpotentials due to its poorer electrical conductivity/contact than the SS cloth. The capacity contributed by carbon paper, if any, should be negligible because the catalytic active VA-NCCF array has significantly lowered the overpotential of the composite electrode compared with the blank carbon paper within the tested capacity range (Figure S11, Supporting Information). Cycling under a deep discharge−charge mode is shown in Figure S12 (Supporting Information). The cell lasted for more than 2000 h. Although the absolute capacity was high, like most other Li−O_2 batteries,[12] the capacity dropped fast, because of the accelerated electrolyte decomposition. In the first five cycles, VA-NCCF presented a capacity retention of 70%.

Further evidence for the good reversibility of the VA-NCCF array catalyst came from an additional test, in which a battery based on the SS-supported VA-NCCF electrode was first run for 100 cycles under a controlled capacity of 1000 mAh g^{-1} per cycle, and then discharged for 20 h (equal to 4000 mAh g^{-1}), followed by charging for 20 h. As seen in Figure S13 (Supporting Information), the discharged fiber was coated by a thick layer of Li_2O_2 (Figure S13a, Supporting Information) while the coral-like fiber structure reappeared after charging (Figure S13b,c, Supporting Information). The coral-like structure seen for the VA-NCCF fiber shown in Figure S13b (Supporting Information) is similar to that of the fiber after the first cycle (Figure 3f), indicating a good rechargeability for the VA-NCCF catalyst over many discharge/charge cycles. It is the interplay of the

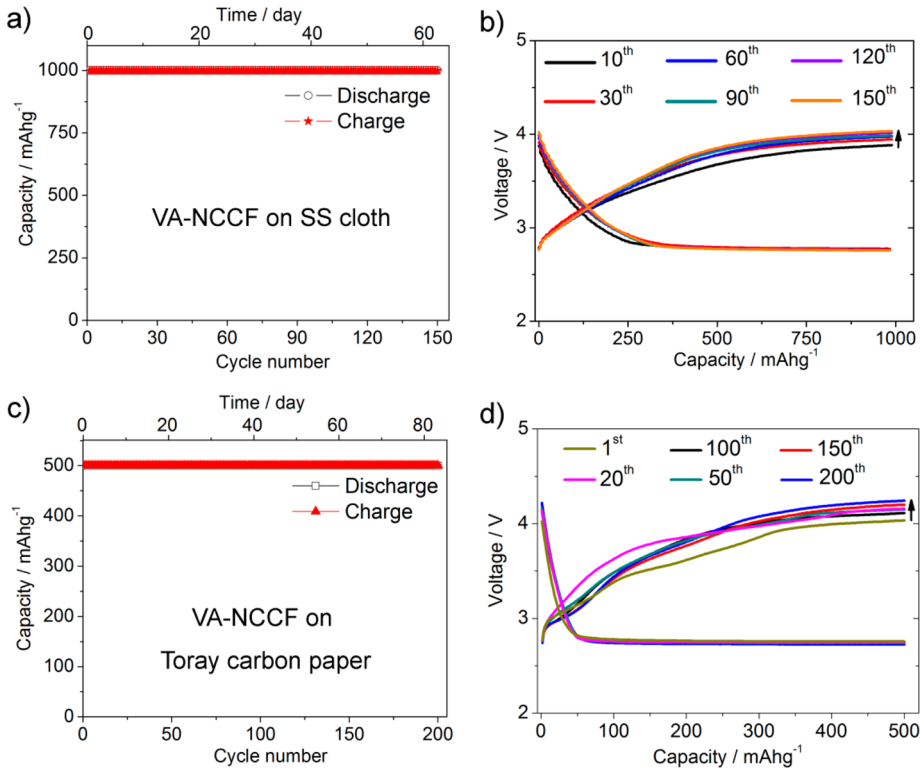

Figure 4. (a) Cycling performance of the VA-NCCF array on the SS cloth substrate. (b) The representative discharge−charge curves from the 10th to 150th cycle for the VA-NCCF electrode. Current density was 500 mA g^{-1}, and a controlled capacity was 1000 mAh g^{-1}. The cell has been working for more than 2 months while the testing is still continuing. (c) Cycling performance of the VA-NCCF electrode on the Toray carbon paper substrate. (d) The representative discharge−charge curves from the 1st to 200th cycle. Current density was 250 mA g^{-1}, and a controlled capacity was 500 mAh g^{-1}.

N-doping-induced high catalytic activity, the coral-like microstructure, and the highly conductive microporous SS cloth support that makes the VA-NCCF oxygen electrode to show the high energy efficiency, low overpotential, and long cycle life.

CONCLUSIONS

In summary, we have developed highly efficient oxygen electrodes for nonaqueous Li−O_2 batteries by using vertically aligned nitrogen-doped coral-like carbon fiber (VA-NCCF) arrays supported with a stainless steel cloth as the current collector. It was demonstrated that these rationally designed VA-NCCF electrodes exhibited an energy efficiency as high as 90% in a full discharge/charge cycle and low overpotential of only 0.3 V between the charge/discharge plateaus. The electrolyte decomposition was minimized due to the low overpotential, and the battery could run for more than 150 cycles with a good reversibility under considerably high specific capacities (up to 1000 mAh g^{-1}) per cycle. The observed outstanding battery performance resulted from multiple factors played together, including the N-doping-induced catalytic activity to lower the charging overpotential for minimizing the electrolyte decomposition and facilitating Li_2O_2 deposition along the VA-NCCF fibers, the unique vertically aligned coral-like fiber structure to provide a large free space for efficient Li_2O_2 deposition and enhanced electron/electrolyte/reactant transport, and the highly conductive microporous SS cloth support with a minimized contact resistance. This work clearly demonstrates that the performance of Li−O_2 batteries could be dramatically improved by using rationally designed oxygen electrodes with well-defined hierarchical structures and heteroatom-doping induced catalytic activities, which represents a significant advance in the research and development of Li−O_2 batteries and other energy devices.

EXPERIMENTAL SECTION

Preparation of Vertically Aligned Nitrogen-Doped Coral-like Carbon Nanofiber Array and Vertically Aligned CNT Array. The pyrolysis of FePc (Iron(II) phthalocyanine, from Sigma Aldrich) was performed for coral-like carbon structure preparation. In a typical experiment, 0.5−0.8 g FePc was loaded into an alumina boat (4 cm × 1 cm × 1 cm), which was then inserted into a 1-in. diameter quartz tube with a silicon wafer as the growth substrate in the middle. After purging the tube furnace (at 850 °C and with 50 cm single heating zone) with 150 mL min^{-1} of helium for 10−15 min, a mixture of helium 50 mL min^{-1} and H_2 100 mL min^{-1} was used as the carry gas for the growth of the vertically aligned coral-like carbon fibers. The growth process was kept for 12−15 min. Vertically aligned

carbon nanotubes (nitrogen-free) were synthesized by pyrolysis of ferrocene according to a previously reported method.[59] A toluene solution of ferrocene (1 wt %) was injected into the tube furnace by using syringe with a 6-in.-long stainless steel needle. Hydrogen gas (40 mL min^{-1}) was used as reduction reagent and argon (100 mL min^{-1}) as carrier gas, and the mixture gas was introduced into the tube furnace at 760 °C. The nanotube growth process took 8–10 min while 3 mL of solution was injected by a syringe.

Oxygen Electrode Preparation and Tests. For the oxygen electrode preparation, the fiber layer was etched off from the Si wafer in HF solution (10%) and then transferred onto a piece of stainless steel (SS) cloth (supersmall particle-filtering stainless steel wire cloth, 304 stainless steel, 200 × 1400 mesh, purchased from McMaster-Carr) or carbon paper (Toray TGP-H-060, purchased from Fuel Cell Store) in deionized water. The electrode was rinsed by deionized water and dried in a vacuum oven (IsoTemp, Model 281A) at 80 °C for 10 h. The catalyst array area is 0.3–0.5 cm^2. The density of a catalyst array was calculated to be 20 $\mu g\ cm^{-2}$ by the array area and the nanofiber weight measured by the microbalance in a thermogravimetric equipment. Thus, the loading on one electrode could be calculated to be 6–10 μg. Surface area could not be measured at the moment because it is too time-consuming to prepare enough materials for BET measurement. And in this work, we are not going to discuss the influence of catalyst surface on battery performance. Thus prepared electrode was assembled into a coin cell (type 2032) with a piece of Li foil as counter electrode and a combination of a piece of glass fiber filter (Whatman) and a piece of porous polymer film (Celgard 2400) as the separator. The electrolyte is 1 M bis(trifluoromethane)sulfonimide lithium salt in tetraethylene glycol dimethyl ether (TEGDME). The cathode side of coin cell was punched with 15 holes (diameter: 1–2 mm) for oxygen transport. The coin cell was assembled in an Ar-filled glovebox (O_2 < 0.1 ppm) and fixed in a homemade plastic bottle. The bottle was filled with high purity oxygen outside of the glovebox. Electrochemical measurements were controlled by a battery cycler (Land, Wuhan, China).

Structure Characterization. Image analysis was conducted on a Hitachi S4500 scanning electron microscope and a FEI Tecnai TF20 FEG transmission electron microscope equipped with a 4k UltraScan CCD camera for digital and a EDAX energy-dispersive X-ray spectrometer (EDX) for elemental analysis. X-ray photoelectron spectroscopic (XPS) measurement was carried out on a VG Microtech ESCA 2000 using a monochromic Al X-ray source (97.9 W, 93.9 eV). Thermogravimetric analyses were performed on TGA (TA500).

Conflict of Interest: The authors declare no competing financial interest.

Acknowledgment. With assistance from Dr. Min Gao, the TEM data were obtained at the (cryo) TEM facility at the Liquid Crystal Institute, Kent State University, supported by the Ohio Research Scholars Program Research Cluster on Surfaces in Advanced Materials. We are thankful for the support from AFOSR (FA9550-12-1-0069; FA9550-12-1-0037), DOD-Army (W911NF-11-1-0209), NSF-AIR (IIP-1343270), NSF (CMMI-1266295), DAGSI, and NSFC-NSF MWN (NSF-DMR 1106160).

Supporting Information Available: Sketch of catalyst growth, extra SEM and TEM images of electrode and catalysts, and extra battery performances of current collectors. This material is available free of charge *via* the Internet at http://pubs.acs.org.

REFERENCES AND NOTES

1. Abraham, K. M.; Jiang, Z. A Polymer Electrolyte-Based Rechargeable Lithium/Oxygen Battery. *J. Electrochem. Soc.* **1996**, *143*, 1–5.
2. Bruce, P. G.; Freunberger, S. A.; Hardwick, L. J.; Tarascon, J. M. Li–O_2 and Li–S Batteries with High Energy Storage. *Nat. Mater.* **2012**, *11*, 19–29.
3. McCloskey, B. D.; Scheffler, R.; Speidel, A.; Bethune, D. S.; Shelby, R. M.; Luntz, A. C. On the Efficacy of Electrocatalysis in Non-Aqueous Li–O_2 Batteries. *J. Am. Chem. Soc.* **2011**, *133*, 18038–18041.
4. Wang, J. J.; Li, Y. L.; Sun, X. L. Challenges and Opportunities of Nanostructured Materials for Aprotic Rechargeable Lithium–Air Batteries. *Nano Energy* **2013**, *2*, 443–467.
5. Wang, Y.; Zheng, D.; Yang, X.; Qu, D. High Rate Oxygen Reduction in Non-Aqueous Electrolytes with the Addition of Perfluorinated Additives. *Energy Environ. Sci.* **2011**, *4*, 3697–3702.
6. Shui, J. L.; Okasinski, J. S.; Kenesei, P.; Dobbs, H. A.; Zhao, D.; Almer, J. D.; Liu, D. J. Reversibility of Anodic Lithium in Rechargeable Lithium–Oxygen Batteries. *Nat. Commun.* **2013**, *4*, 2255.
7. Zhang, T.; Zhou, H. S. A Reversible Long-Life Lithium–Air Battery in Ambient Air. *Nat. Commun.* **2013**, *4*, 1817.
8. Hassoun, J.; Jung, H. G.; Lee, D. J.; Park, J. B.; Amine, K.; Sun, Y. K.; Scrosati, B. A Metal-Free, Lithium–Ion Oxygen Battery: A Step Forward to Safety in Lithium–Air Batteries. *Nano Lett.* **2012**, *12*, 5775–5779.
9. Lu, Y. C.; Xu, Z. C.; Gasteiger, H. A.; Chen, S.; Hamad-Schifferli, K.; Shao-Horn, Y. Platinum-Gold Nanoparticles: A Highly Active Bifunctional Electrocatalyst for Rechargeable Lithium–Air Batteries. *J. Am. Chem. Soc.* **2010**, *132*, 12170–12171.
10. Shui, J. L.; Okasinski, J. S.; Chen, C.; Almer, J. D.; Liu, D. J. In Operando Spatiotemporal Study of Li_2O_2 Grain Growth and Its Distribution Inside Operating Li–O_2 Batteries. *ChemSusChem* **2014**, *7*, 543–548.
11. Ogasawara, T.; Débart, A.; Holzapfel, M.; Novák, P.; Bruce, P. G. Rechargeable Li_2O_2 Electrode for Lithium Batteries. *J. Am. Chem. Soc.* **2006**, *128*, 1390–1393.
12. Freunberger, S. A.; Chen, Y. H.; Drewett, N. E.; Hardwick, L. J.; Bardé, F.; Bruce, P. G. The Lithium–Oxygen Battery with Ether-Based Electrolytes. *Angew. Chem., Int. Ed.* **2011**, *50*, 8609–8613.
13. Jung, H. G.; Hassoun, J.; Park, J. B.; Sun, Y. K.; Scrosati, B. An Improved High-Performance Lithium–Air Battery. *Nat. Chem.* **2012**, *4*, 579–585.
14. Freunberger, S. A.; Chen, Y. H.; Peng, Z. Q.; Griffin, J. M.; Hardwick, L. J.; Bardé, F.; Novák, P.; Bruce, P. G. Reactions in the Rechargeable Lithium–O_2 Battery with Alkyl Carbonate Electrolytes. *J. Am. Chem. Soc.* **2011**, *133*, 8040–8047.
15. McCloskey, B. D.; Bethune, D. S.; Shelby, R. M.; Girishkumar, G.; Luntz, A. C. Solvents' Critical Rope in Nonaqueous Lithium–Oxygen Battery Electrochemistry. *J. Phys. Chem. Lett.* **2011**, *2*, 1161–1166.
16. Xu, W.; Xu, K.; Viswanathan, V. V.; Towne, S. A.; Hardy, J. S.; Xiao, J.; Nie, Z. M.; Hu, D. H.; Wang, D. Y.; Zhang, J. G. Reaction Mechanisms for the Limited Reversibility of Li–O_2 Chemistry in Organic Carbonate Electrolytes. *J. Power Sources* **2011**, *196*, 9631–9639.
17. Shui, J. L.; Okasinski, J. S.; Zhao, D.; Almer, J. D.; Liu, D. J. Microfocused X-ray Study on Precipitate Formation in the Separator Region of Nonaqueous Li–O_2 Batteries. *ChemSusChem* **2012**, *5*, 2421–2426.
18. Shui, J. L.; Wang, H. H.; Liu, D. J. Degradation and Revival of Li–O_2 Battery Cathode. *Electrochem. Commun.* **2013**, *34*, 45–47.
19. Thotiyl, M. M. O.; Freunberger, S. A.; Peng, Z. Q.; Bruce, P. G. The Carbon Electrode in Nonaqueous Li–O_2 Cells. *J. Am. Chem. Soc.* **2013**, *135*, 494–500.
20. Elia, G. A.; Park, J. B.; Scrosati, B.; Sun, Y. K.; Hassoun, J. Investigation of the Carbon Electrode Changes During Lithium Oxygen Cell Operation in a Tetraglyme-Based Electrolyte. *Electrochem. Commun.* **2013**, *34*, 250–253.
21. McCloskey, B. D.; Speidel, A.; Scheffler, R.; Miller, D. C.; Viswanathan, V.; Hummelshoj, J. S.; Norskov, J. K.; Luntz, A. C. Twin Problems of Interfacial Carbonate Formation in Nonaqueous Li–O_2 Batteries. *J. Phys. Chem. Lett.* **2012**, *3*, 997–1001.
22. Gallant, B. M.; Mitchell, R. R.; Kwabi, D. G.; Zhou, J. G.; Zuin, L.; Thompson, C. V.; Shao-Horn, Y. Chemical and Morphological Changes of Li–O_2 Battery Electrodes upon Cycling. *J. Phys. Chem. C* **2012**, *116*, 20800–20805.
23. Itkis, D. M.; Semenenko, D. A.; Kataev, E. Y.; Belova, A. I.; Neudachina, V. S.; Sirotina, A. P.; Havecker, M.; Teschner, D.; Knop-Gericke, A.; Dudin, P.; *et al.* Reactivity of Carbon in Lithium–Oxygen Battery Positive Electrodes. *Nano Lett.* **2013**, *13*, 4697–4701.

24. Chen, Y. H.; Freunberger, S. A.; Peng, Z. Q.; Fontaine, O.; Bruce, P. G. Charging a Li−O_2 Battery Using a Redox Mediator. *Nat. Chem.* **2013**, *5*, 489–494.
25. Jung, H. G.; Kim, H. S.; Park, J. B.; Oh, I. H.; Hassoun, J.; Yoon, C. S.; Scrosati, B.; Sun, Y. K. A Transmission Electron Microscopy Study of the Electrochemical Process of Lithium−Oxygen Cells. *Nano Lett.* **2012**, *12*, 4333–4335.
26. Cui, Y. M.; Wen, Z. Y.; Liang, X.; Lu, Y.; Jin, J.; Wu, M. F.; Wu, X. W. A Tubular Polypyrrole Based Air Electrode with Improved O_2 Diffusivity for Li−O_2 Batteries. *Energy Environ. Sci.* **2012**, *5*, 7893–7897.
27. Zhong, L.; Mitchell, R. R.; Liu, Y.; Gallant, B. M.; Thompson, C. V.; Huang, J. Y.; Mao, S. X.; Shao-Horn, Y. *In Situ* Transmission Electron Microscopy Observations of Electrochemical Oxidation of Li_2O_2. *Nano Lett.* **2013**, *13*, 2209–2214.
28. Li, F. J.; Ohnishi, R.; Yamada, Y.; Kubota, J.; Domen, K.; Yamada, A.; Zhou, H. S. Carbon Supported TiN Nanoparticles: an Efficient Bifunctional Catalyst for Non-aqueous Li−O_2 Batteries. *Chem. Commun.* **2013**, *49*, 1175–1177.
29. Sun, B.; Munroe, P.; Wang, G. X. Ruthenium Nanocrystals as Cathode Catalysts for Lithium−Oxygen Batteries with a Superior Performance. *Sci. Rep.* **2013**, *3*, 2247.
30. Peng, Z. Q.; Freunberger, S. A.; Chen, Y. H.; Bruce, P. G. A Reversible and Higher-Rate Li−O_2 Battery. *Science* **2012**, *337*, 563–566.
31. Wang, L.; Zhao, X.; Lu, Y. H.; Xu, M. W.; Zhang, D. W.; Ruoff, R. S.; Stevenson, K. J.; Goodenough, J. B. $CoMn_2O_4$ Spinel Nanoparticles Grown on Graphene as Bifunctional Catalyst for Lithium−Air Batteries. *J. Electrochem. Soc.* **2011**, *158*, A1379–A1382.
32. Li, Y.; Wang, J.; Li, X.; Geng, D.; Banis, M. N.; Li, R.; Sun, X. Nitrogen-Doped Graphene Nanosheets as Cathode Materials with Excellent Electrocatalytic Activity for High Capacity Lithium−Oxygen Batteries. *Electrochem. Commun.* **2012**, *18*, 12–15.
33. Lei, Y.; Lu, J.; Luo, X.; Wu, T.; Du, P.; Zhang, X.; Ren, Y.; Wen, J.; Miller, D. J.; Miller, J. T.; *et al.* Synthesis of Porous Carbon Supported Palladium Nanoparticle Catalysts by Atomic Layer Deposition: Application for Rechargeable Lithium−O_2 Battery. *Nano Lett.* **2013**, *13*, 4182–4189.
34. Ryu, W.-H.; Yoon, T.-H.; Song, S. H.; Jeon, S.; Park, Y.-J.; Kim, I.-D. Bifunctional Composite Catalysts Using Co_3O_4 Nanofibers Immobilized on Nonoxidized Graphene Nanoflakes for High-Capacity and Long-Cycle Li−O_2 Batteries. *Nano Lett.* **2013**, *13*, 4190–4197.
35. Wang, Z. L.; Xu, D.; Xu, J. J.; Zhang, L. L.; Zhang, X. B. Graphene Oxide Gel-Derived, Free-Standing, Hierarchically Porous Carbon for High-Capacity and High-Rate Rechargeable Li−O_2 Batteries. *Adv. Funct. Mater.* **2012**, *22*, 3699–3705.
36. Lim, H. D.; Park, K. Y.; Song, H.; Jang, E. Y.; Gwon, H.; Kim, J.; Kim, Y. H.; Lima, M. D.; Robles, R. O.; Lepro, X.; *et al.* Enhanced Power and Rechargeability of a Li−O_2 Battery Based on a Hierarchical-Fibril CNT Electrode. *Adv. Mater.* **2013**, *25*, 1348–1352.
37. Mitchell, R. R.; Gallant, B. M.; Thompson, C. V.; Shao-Horn, Y. All-Carbon-Nanofiber Electrodes for High-Energy Rechargeable Li−O_2 Batteries. *Energy Environ. Sci.* **2011**, *4*, 2952–2958.
38. Zhang, G. Q.; Zheng, J. P.; Liang, R.; Zhang, C.; Wang, B.; Au, M.; Hendrickson, M.; Plichta, E. J. Alpha-MnO_2/Carbon Nanotube/Carbon Nanofiber Composite Catalytic Air Electrodes for Rechargeable Lithium−Air Batteries. *J. Electrochem. Soc.* **2011**, *158*, A822–A827.
39. Zhang, G. Q.; Zheng, J. P.; Liang, R.; Zhang, C.; Wang, B.; Hendrickson, M.; Plichta, E. J. Lithium−Air Batteries Using SWNT/CNF Buckypapers as Air Electrodes. *J. Electrochem. Soc.* **2010**, *157*, A953–A956.
40. Yoon, T. H.; Park, Y. J. Carbon Nanotube/Co_3O_4 Composite for Air Electrode of Lithium−Air Battery. *Nanoscale Res. Lett.* **2012**, *7*, 1–4.
41. Zhang, T.; Zhou, H. S. From Li−O_2 to Li−Air Batteries: Carbon Nanotubes/Ionic Liquid Gels with a Tricontinuous Passage of Electrons, Ions, and Oxygen. *Angew. Chem., Int. Ed.* **2012**, *51*, 11062–11067.
42. Jian, Z. L.; Liu, P.; Li, F. J.; He, P.; Guo, X. W.; Chen, M. W.; Zhou, H. S. Core-Shell-Structured CNT@RuO_2 Composite as a High-Performance Cathode Catalyst for Rechargeable Li−O_2 Batteries. *Angew. Chem., Int. Ed.* **2014**, *53*, 442–446.
43. Yilmaz, E.; Yogi, C.; Yamanaka, K.; Ohta, T.; Byon, H. R. Promoting Formation of Noncrystalline Li_2O_2 in the Li−O_2 Battery with RuO_2 Nanoparticles. *Nano Lett.* **2013**, *13*, 4679–4684.
44. Shen, Y.; Sun, D.; Yu, L.; Zhang, W.; Shang, Y. Y.; Tang, H. R.; Wu, J. F.; Cao, A. Y.; Huang, Y. H. A High-Capacity Lithium−Air Battery with Pd Modified Carbon Nanotube Sponge Cathode Working in Regular Air. *Carbon* **2013**, *62*, 288–295.
45. Lim, H. D.; Song, H.; Gwon, H.; Park, K. Y.; Kim, J.; Bae, Y.; Kim, H.; Jung, S. K.; Kim, T.; Kim, Y. H.; *et al.* A New Catalyst-Embedded Hierarchical Air Electrode for High-Performance Li−O_2 Batteries. *Energy Environ. Sci.* **2013**, *6*, 3570–3575.
46. Oh, D.; Qi, J. F.; Lu, Y. C.; Zhang, Y.; Shao-Horn, Y.; Belcher, A. M. Biologically Enhanced Cathode Design for Improved Capacity and Cycle Life for Lithium−Oxygen Batteries. *Nat. Commun.* **2013**, *4*, 2756.
47. Shui, J. L.; Karan, N. K.; Balasubramanian, M.; Li, S. Y.; Liu, D. J. Fe/N/C Composite in Li−O_2 Battery: Studies of Catalytic Structure and Activity toward Oxygen Evolution Reaction. *J. Am. Chem. Soc.* **2012**, *134*, 16654–16661.
48. Jung, H. G.; Jeong, Y. S.; Park, J. B.; Sun, Y. K.; Scrosati, B.; Lee, Y. J. Ruthenium-Based Electrocatalysts Supported on Reduced Graphene Oxide for Lithium−Air Batteries. *ACS Nano* **2013**, *7*, 3532–3539.
49. Black, R.; Oh, S. H.; Lee, J. H.; Yim, T.; Adams, B.; Nazar, L. F. Screening for Superoxide Reactivity in Li−O_2 Batteries: Effect on Li_2O_2/LiOH Crystallization. *J. Am. Chem. Soc.* **2012**, *134*, 2902–2905.
50. Wang, S. Y.; Iyyamperumal, E.; Roy, A.; Xue, Y. H.; Yu, D. S.; Dai, L. M. Vertically Aligned BCN Nanotubes as Efficient Metal-Free Electrocatalysts for the Oxygen Reduction Reaction: A Synergetic Effect by Co-Doping with Boron and Nitrogen. *Angew. Chem., Int. Ed.* **2011**, *50*, 11756–11760.
51. Gong, K. P.; Du, F.; Xia, Z. H.; Durstock, M.; Dai, L. M. Nitrogen-Doped Carbon Nanotube Arrays with High Electrocatalytic Activity for Oxygen Reduction. *Science* **2009**, *323*, 760–764.
52. Lefèvre, M.; Proietti, E.; Jaouen, F.; Dodelet, J. P. Iron-Based Catalysts with Improved Oxygen Reduction Activity in Polymer Electrolyte Fuel Cells. *Science* **2009**, *324*, 71–74.
53. Yu, D. S.; Zhang, Q.; Dai, L. M. Highly Efficient Metal-Free Growth of Nitrogen-Doped Single-Walled Carbon Nanotubes on Plasma-Etched Substrates for Oxygen Reduction. *J. Am. Chem. Soc.* **2010**, *132*, 15127–15129.
54. Wu, G.; Mack, N. H.; Gao, W.; Ma, S. G.; Zhong, R. Q.; Han, J. T.; Baldwin, J. K.; Zelenay, P. Nitrogen Doped Graphene-Rich Catalysts Derived from Heteroatom Polymers for Oxygen Reduction in Nonaqueous Lithium−O_2 Battery Cathodes. *ACS Nano* **2012**, *6*, 9764–9776.
55. Zhu, D.; Zhang, L.; Song, M.; Wang, X. F.; Chen, Y. G. An *In Situ* Formed Pd Nanolayer as a Bifunctional Catalyst for Li−Air Batteries in Ambient or Simulated Air. *Chem. Commun.* **2013**, *49*, 9573–9575.
56. Zhai, D. Y.; Wang, H. H.; Yang, J. B.; Lau, K. C.; Li, K. X.; Amine, K.; Curtiss, L. A. Disproportionation in Li−O_2 Batteries Based on a Large Surface Area Carbon Cathode. *J. Am. Chem. Soc.* **2013**, *135*, 15364–15372.
57. Adams, B. D.; Radtke, C.; Black, R.; Trudeau, M. L.; Zaghib, K.; Nazar, L. F. Current Density Dependence of Peroxide Formation in the Li−O_2 Battery and its Effect on Charge. *Energy Environ. Sci.* **2013**, *6*, 1772–1778.
58. Horstmann, B.; Gallant, B.; Mitchell, R.; Bessler, W. G.; Shao-Horn, Y.; Bazant, M. Z. Rate-Dependent Morphology of Li_2O_2 Growth in Li−O_2 Batteries. *J. Phys. Chem. Lett.* **2013**, *4*, 4217–4222.
59. Wei, B. Q.; Vajtai, R.; Jung, Y.; Ward, J.; Zhang, R.; Ramanath, G.; Ajayan, P. M. Organized Assembly of Carbon Nanotubes. *Nature* **2002**, *416*, 495–496.